Hindawi Publishing Corporation
International Journal of Corrosion
Volume 2011, Article ID 824676, 10 pages
doi:10.1155/2011/824676

Research Article

Breakdown and Evolution of the Protective Oxide Scales of AISI 304 and AISI 316 Stainless Steels under High-Temperature Oxidation

K. A. Habib, M. S. Damra, J. J. Saura, I. Cervera, and J. Bellés

Departamento de Ingeniería de Sistemas Industriales y Diseño, Universitat Jaume I, 12071 Castellón, Spain

Correspondence should be addressed to K. A. Habib, razzaq@esid.uji.es

Received 11 April 2011; Accepted 15 June 2011

Academic Editor: Ravin Kumar Dayal

The failure of the protective oxide scales of AISI 304 and AISI 316 stainless steels has been studied and compared at 1,000°C in synthetic air. First, the isothermal thermogravimetric curves of both stainless steels were plotted to determine the time needed to reach the breakdown point. The different resistance of each stainless steel was interpreted on the basis of the nature of the crystalline phases formed, the morphology, and the surface structure as well as the cross-section structure of the oxidation products. The weight gain of AISI 304 stainless steel was about 8 times greater than that of AISI 316 stainless steel, and AISI 316 stainless steel reached the breakdown point about 40 times more slowly than AISI 304 stainless steel. In both stainless steels, reaching the breakdown point meant the loss of the protective oxide scale of Cr_2O_3, but whereas in AISI 304 stainless steel the Cr_2O_3 scale totally disappeared and exclusively Fe_2O_3 was formed, in AISI 316 stainless steel some Cr_2O_3 persisted and Fe_3O_4 was mainly formed, which means that AISI 316 stainless steel is more resistant to oxidation after the breakdown.

1. Introduction

Austenitic stainless steels can be found in a wide range of applications, such as superheaters, reheater tubes, turbine blades, and equipment components which are subjected to thermal fluctuations under normal operation conditions; therefore, protection against degradation caused by high temperatures is necessary. This protection can be achieved thanks to the formation of a protective scale of Cr_2O_3 which slows down the degradation of the metal substrate. This protective scale is maintained under mildly oxidizing conditions, with its growth kinetics approximating a parabolic relationship until 900°C. Under severe conditions of oxidation or at temperatures above 900°C, a fast increase of scale growth may occur; this is known as breakdown and depends on the material, the oxidation environment, the temperature, and the time. This breakdown corresponds to the formation of a duplex layer consisting of an inner scale of a spinel and an exterior scale of Fe_2O_3. Depending on the material and the environment, this fast oxidation can continue or, on the contrary, the oxidation velocity can decrease [1–5]. There has been little work on the breakdown and the subsequent degradation of these types of stainless steels at 1,000°C. At temperatures above 800°C, the evaporation of chromium can occur, and this tends to convert the 50–200 μm thick protective scale of Cr_2O_3 which was formed initially to a less protective scale, rich in iron oxides (Fe_2O_3/Fe_3O_4) and less thick [6]. For the interpretation of the breakdown failure mechanism, there are two recommended possibilities: "chemical failure" of the protective Cr_2O_3 scale and "mechanical failure" of the protective Cr_2O_3 scale [7].

High-temperature oxidation of stainless steels has already been studied in the literature; however, the objective of this study was to evaluate and compare the characteristics of the breakdown at 1,000°C in a synthetic air environment and the products formed in AISI 304 and AISI 316 stainless steels, emphasizing the differences found.

2. Experimental Procedures

Two stainless steels, AISI 304 and AISI 316, were investigated at 1,000°C in a synthetic air environment. Table 1 shows the chemical composition of the stainless steels used as the metal base.

Table 1: The chemical composition of the stainless steel used as metal base.

AISI 304													
Cr	Ni	Mn	Cu	Co	Mo	Si	C	P	S	N	V	Nb	Ti
18.21	8.18	1.51	0.30	0.12	0.21	0.42	0.065	0.032	0.002	0.0389	0.083	0.009	0.003
AISI 316													
Cr	Ni	Mn	Cu	Co	Mo	Si	C	P	S	N	V	Nb	Ti
17.02	10.7	1.17	0.41	0.17	2.8	0.32	0.03	0.029	0.006	0.0473	0.078	0.014	0.022

Tests specimens of $20 \times 10 \times 1\,\text{mm}^3$ were cut from cold-rolled sheet in the austenitic tempering state (hyper-tempering), and all sides were ground to SiC no. 600. The top surfaces of the base metal sample were polished with diamond paste in three sequential steps, namely, 6-, 3- and 1-μm-grade diamond lapping to achieve a mirror-like finish. Prior to oxidation, the samples were ultrasonically degreased in acetone for 15 min and cleaned with ethanol.

The samples were isothermally oxidized in a thermobalance (TGA 92-16 Setaram) with synthetic air (1-bar pressure) from room temperature to 1,000°C at a rate of $40^\circ\text{C}\,\text{min}^{-1}$, held for 100 h, and then cooled to room temperature at a rate of $40^\circ\text{C}\,\text{min}^{-1}$.

The techniques used to characterize the structure and the composition of the oxidation products formed included optical metallography, X-ray diffraction (XRD), scanning electron microscopy (SEM), and energy dispersive X-ray (EDX) analysis.

3. Results and Discussion

3.1. Thermogravimetric Results. It was very important to carry out the experiment on the stainless steels at 1,000°C to reach the breakdown point.

Figure 1 shows the kinetics of the oxidation of AISI 304 stainless steel. The sample reaches the breakdown state after almost 2 h of oxidation. The curve in Figure 1 passes from the parabolic case to the linear case. The severity of the oxidation could be observed on the steel surface.

The temperature of 1,000°C was critical and crucial in the running tests because at 900°C the oxidation behaviour was parabolic [8].

The stresses start accumulating with the oxide growth process as the weight increases due to oxidation. However, at a certain point, the scale thickness is unable to bear the increased stress and the stress is released. The release of stress may be due to either cracking in the scale or creep of the substrate metal (base metal) [1–5]. Figure 1 shows in our case the curve before and after the breakdown. After approximately 8,000 s, or 2 h, the transition state started and the curve changed from parabolic to linear, indicating that the protective layer started to break and the oxidation increased. The mass gain obtained was $0.1569\,\text{mg}\,\text{mm}^{-2}$.

The oxidation behaviour of AISI 316 stainless steel at 1,000°C is shown in Figure 2. The test sample reached the breakdown limit after about 80 h. The oxidation on the sample surface was less severe than that for AISI 304 stainless steel.

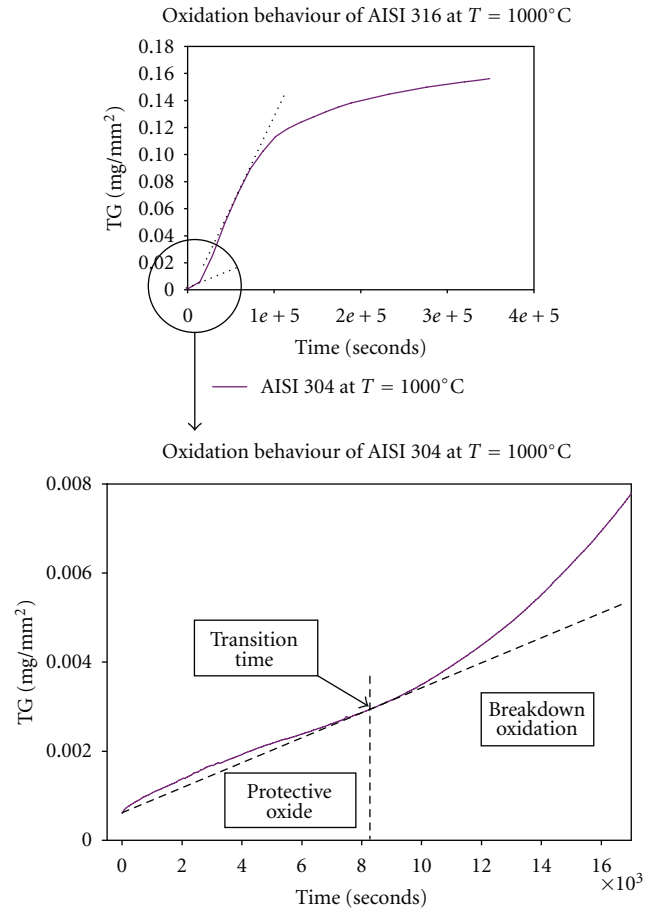

Figure 1: The scale breakdown obtained of AISI 304 at $T = 1000^\circ\text{C}$ in synthetic air.

The temperature of 1,000°C was critical and crucial in the running tests because at 900°C the oxidation behaviour was parabolic [8]. The mass gain obtained was $0.0209\,\text{mg}\,\text{mm}^{-2}$.

4. Surface Characterization

4.1. X-Ray Diffraction Analysis. The crystalline phases, oxides obtained after corrosion, were analyzed by XRD, using a D5000D diffractometer from Siemens (Germany), employed at ambient temperature with a scan of intensity versus diffraction angle between 5° and 70° (step size of 0.050°, scanner velocity of 3 s per step) using copper K_α radiation ($\lambda = 1.5406$Å), a voltage of 40 kV, and a 30-mA filament current.

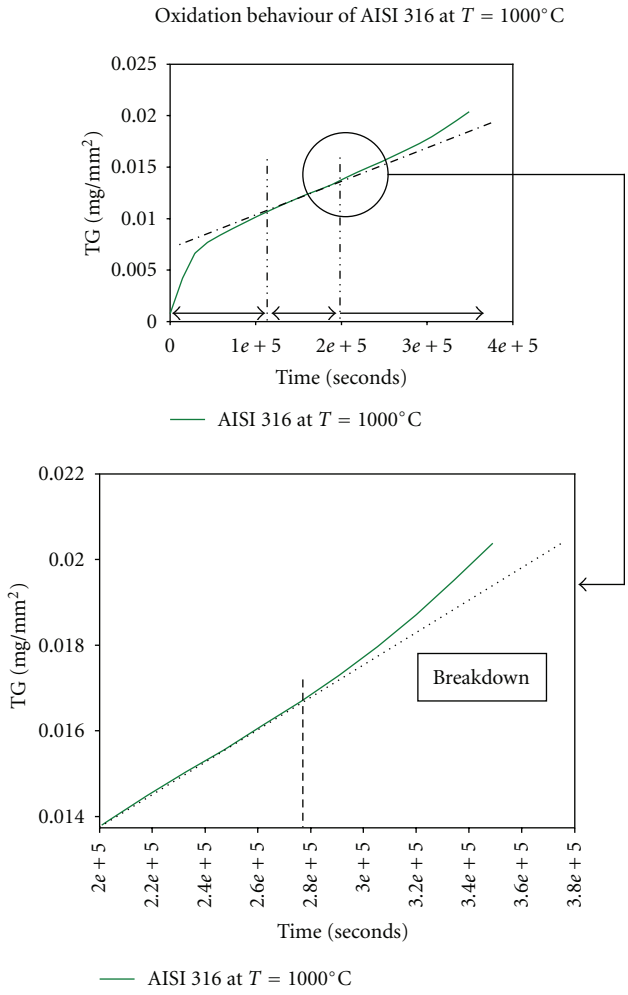

Figure 2: The scale breakdown obtained of AISI 316 at $T = 1000°C$ in synthetic air.

X-ray characterization of the surface of AISI 304 stainless steel (Figure 3) shows that Fe_2O_3 (haematite) and a mixture of oxides of iron and chromium are the main compounds produced by the oxidation. No nickel-bearing phases could be identified at 1,000°C. In addition, no protective scale of Cr_2O_3 was found. This result is in good agreement with the literature [1–5]: when there is no protective oxide scale, such as Cr_2O_3, because it has been destroyed, breakdown occurs.

X-ray characterization of the surface of AISI 316 stainless steel (Figure 4) shows two different phases of Fe_3O_4 (magnetite) and a chromium iron oxide. No protective scale of Cr_2O_3 was found. This result is in good agreement with the literature: when there is no protective oxide scale, because it has been destroyed, breakdown occurs.

5. Scanning Electron Microscopy

Figure 5 shows SEM micrographs of the sample surface at different magnifications, ×20, ×100, and ×400, respectively, with the objective to distinguish between two different zones: the island formed and next closed zone divided by the border line. The oxidation is spread irregularly and can be seen clearly as scattered islands above the surface.

The results of the EDX microanalysis of the islands and the area next to the islands are shown in Table 2. The islands are rich in Fe_2O_3 and contain some MnO. A very small amount of iron chromium oxide was detected. These islands are full of iron oxide after the breakdown, and because no Cr_2O_3 was detected there is no protection. This finding coincides with the finding from the XRD analysis.

The SEM micrograph of AISI 316 stainless steel demonstrates that it formed a heterogeneous oxide layer after the full oxidation run. Grey and dark-grey scales were found to have grown as a blanket containing a few large nodules and numerous small nodules, as can be seen from Figure 6.

Two different zones were detected: large and small nodules (zone A) and the damaged Cr_2O_3 layer (zone B), the EDX analysis data for which are given in Table 3. The nodules had a porous structure, where the diffusion of oxygen may easily proceed. On the other hand, the damaged Cr_2O_3 layer is less porous than the nodules but is not totally compact.

The damaged Cr_2O_3 layer is adjacent to the nodules and it has a crystalline structure, as shown in Figure 6(d).

The protective effect of Cr_2O_3 is limited to around 1,000°C owing to the formation of volatile CrO_3. When mechanical failure of the initially formed passive layer takes place, this leads to the nucleation and growth of oxide nodules via short circuits.

Cr_2O_3 was formed at the beginning, but as oxidation proceeded iron may have begun to oxidize because depletion of chromium in the bulk alloy may have taken place [9]. After the transition period, faster kinetics was found, probably because of the incorporation of iron into the oxide scale. Between 48 and 90 h, transition of oxides grown at high temperature from the protective state to the breakdown state takes place. Therefore, the oxidation rate increases with increasing time, probably corresponding to the formation of iron oxides.

The formation of iron oxides could be due to the depletion of chromium on the surface, and because of volatilization of CrO_3, subsequent depletion of chromium occurs. The oxidation of Cr_2O_3 to CrO_3, which is volatile, occurs at about 950°C [10–13].

The breakdown of AISI 316 stainless steel is due to the formation of porous nodules of Fe_3O_4 and oxides of iron and chromium, the same way as scales were formed (the damaged Cr_2O_3 layer) by a mixture of Fe_2O_3 and oxides of iron and chromium. These oxidation products totally cover the substrate, unlike in AISI 304 stainless steel, which formed islands of Fe_2O_3 after breakdown with less protection capacity than Fe_3O_4, the formation of which can probably explain the breakdown delay in the case of AISI 316 stainless steel with respect to AISI 304 stainless steel.

6. Cross-Section Characterization

Figure 7 shows the cross-section of AISI 304 stainless steel oxidized at 1,000°C for 100 h. The oxidation was severe in this test since the sample reached the breakdown limit. Three

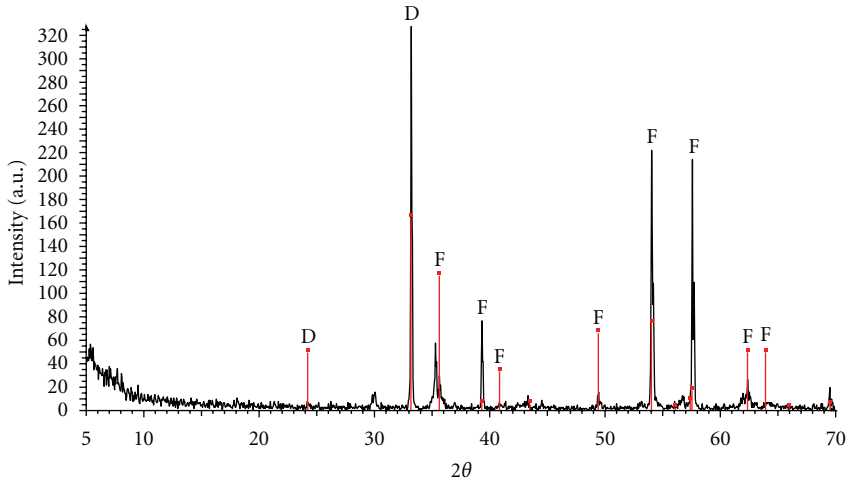

Figure 3: X-ray diffraction image for AISI 304 stainless steel oxidized in synthetic air at $T = 1000°C$.

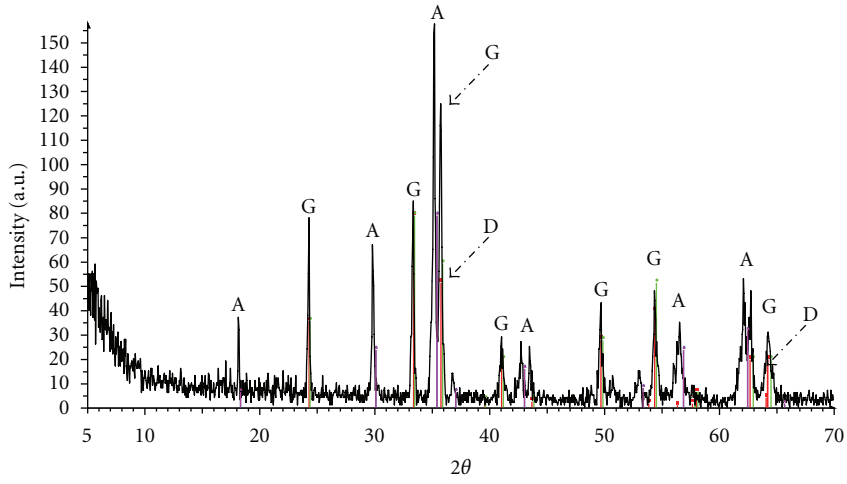

Figure 4: X-ray diffraction image for AISI 316 stainless steel oxidized in synthetic air at $T = 1000°C$.

significant areas will be studied here: the substrate-oxide area, the interior oxidation, and the exterior oxide scales.

EDX spectroscopic data for the oxides from the three significant areas are presented in Table 4.

Figure 7(b) shows the substrate-oxide area and the interface line between the substrate and the oxide. The deterioration due to oxidation was spread towards the base metal. It seems that the oxides are not continuous and do not adhere well to the substrate. There are many microcracks between the substrate and the interior oxide, and there are voids in both of them. The EDX analysis of the substrate oxides found (Table 4) demonstrates a high content of Cr_2O_3 (70.57%) and also of Fe_3O_4 (28.54%) and a negligible amount of NiO. These oxides are considered to be ones found in the initial process of oxidation under the oxide layer.

Figure 7(c) shows the internal oxidation area: it is of nonuniform thickness and is composed of alternate layers of light and dark colour, both containing voids, and pores are evidenced by the black colour. This interior layer is uniformly adhered to the base metal. The EDX analysis of the oxides found (Table 4) demonstrates a moderate content of Cr_2O_3 (40.34%) and also of Fe_3O_4 (46.97%) and a greater content of NiO (12.69%).

Figure 7(d) shows the external oxidation area: it is of uniform thickness, approximately 130 μm, and is separated by a crack in the interior oxidation layer. This area consists of

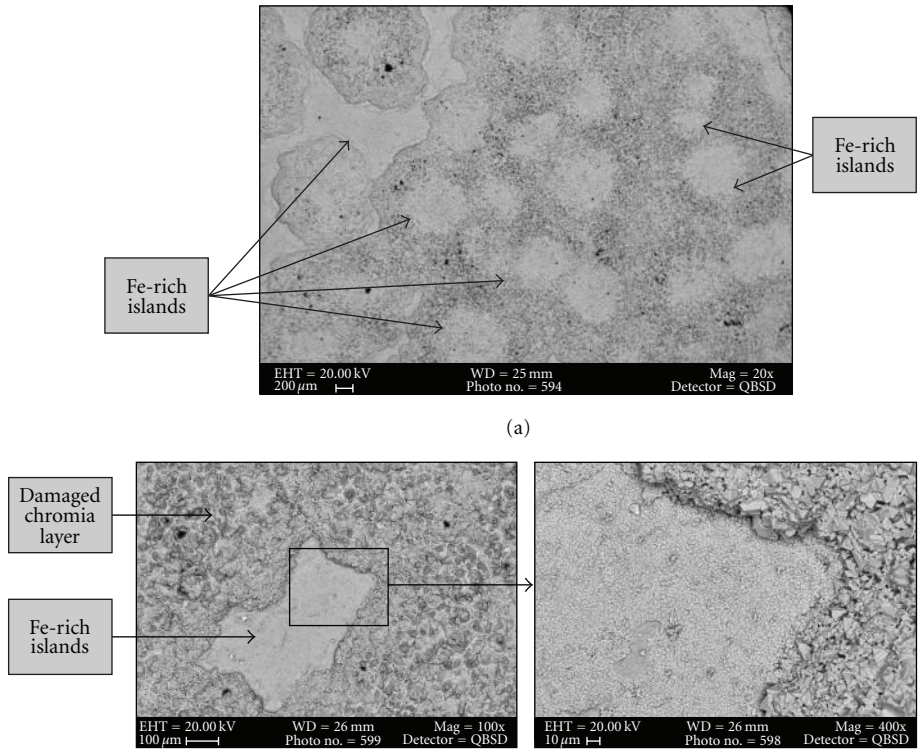

Figure 5: General aspect of the oxidized AISI 304 surface at $T = 1000^{\circ}$C and after 100 hours, (a) Fe-rich islands at magnification 20x, (b) border line of an island at magnifications 100x and (c) 400x.

Table 2: EDX spectra results of islands and next to islands for AISI 304 at $T = 1000^{\circ}$C.

Oxide	Islands %	Next to islands %
Fe_2O_3	93.56	26.21
NiO	1.27	2.29
MnO	4.23	20.08
(Fe, Cr)O	0.94	51.42
Total	100.00	100.00

Table 3: EDX spectra results of large and small nodules for AISI 316 at $T = 1000^{\circ}$C.

Oxide	Nodule (zone A) %	Damaged chromia layer (zone B) %
Fe_3O_4	87.23	—
Fe_2O_3	—	14.78
(Ni, Mo, C)O	—	2.87
MnO	2.27	14.23
(Cr, Fe)O	10.5	67.99
Total	100.00	100.00

two different areas: a light-grey area and a dark-grey area. Compared with the internal oxidation area, this oxide-gas interface has fewer voids and pores. The EDX analysis of the oxides found (Table 4) demonstrates a low content of Cr_2O_3 (6.82%), a high content of Fe_2O_3 (92.71%), and a negligible amount of NiO (0.47%). Fe_3O_4 has totally disappeared.

In conclusion, the breakdown reveals, firstly, cracks in the interior oxide, that is, between the interior oxide and the exterior oxide, and, secondly, the poor Cr_2O_3 content of the exterior oxide layer.

Figure 8 shows the X-ray mapping of the elements according to the line chosen to cross through all the oxide scales formed to give a general concept of the diffusion of the elements during the oxidation. According to Figure 8(b), the oxygen content of the oxides remains high, but the content is greater in the interior oxide layer. The oxides of the interior layer correspond to NiO and Cr_2O_3, the content of which decreases as it becomes nearer to the interface between the inner and outer oxides. Iron generally diffused towards the exterior oxide layer; therefore, the breakdown became manifest in addition to the cracks and the poor Cr_2O_3 layer. Iron was mainly concentrated in the exterior oxide layer and in the form of Fe_2O_3.

Figure 9 shows a SEM image of the cross-section of AISI 316 stainless steel after 100 h of oxidation at 1,000°C. A thin oxidation scale between 2 and 12 μm thick was formed; some blankets and nodules of oxidation formed above the scale surface, and cracks in the blankets and intrusions in the substrate were also formed.

The results of the analysis of the oxides from the three significant areas are shown in Table 5.

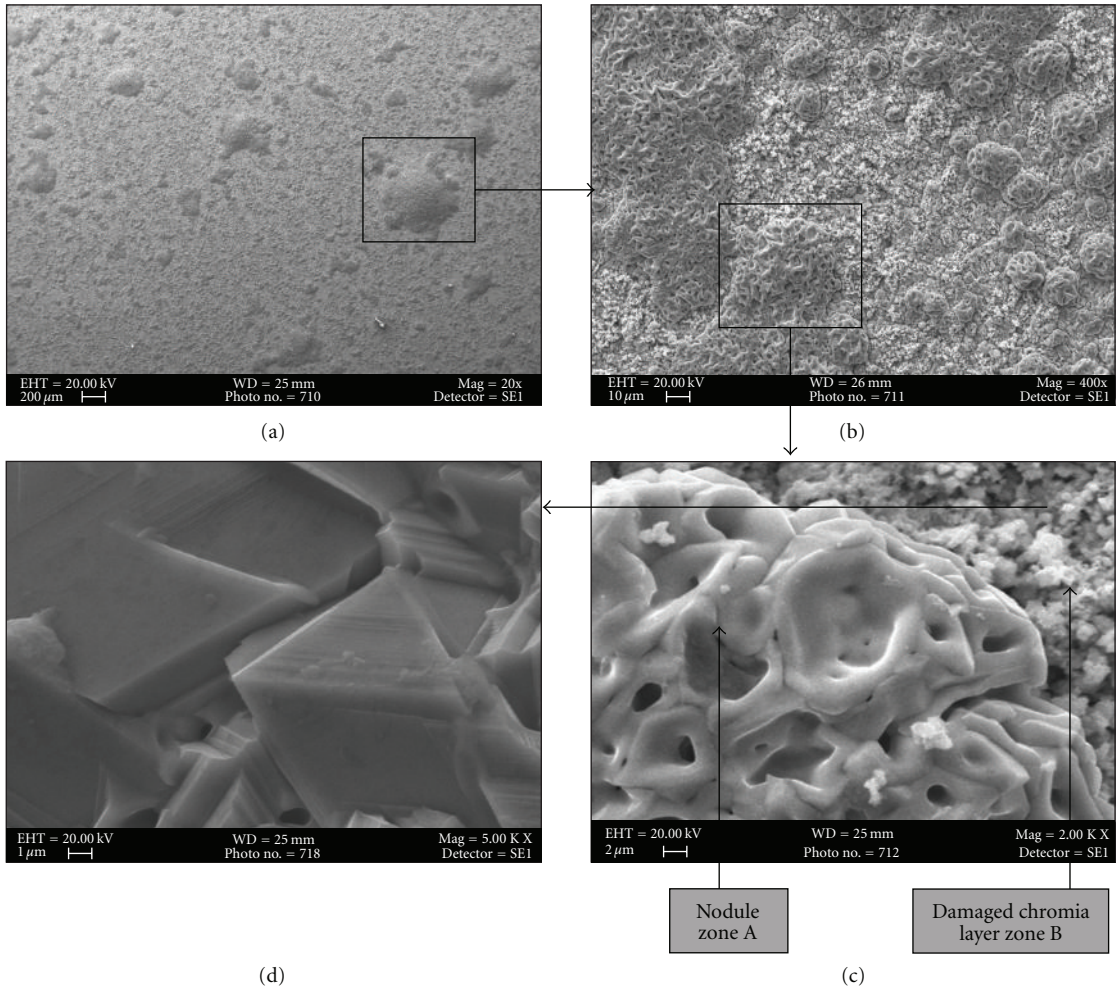

Figure 6: SEM micrograph of the surface of AISI 316 oxidized at 1000°C for 100 hours; (a) SEM image of the whole surface at magnification 20x, (b) SEM image at magnification 400x, (c) SEM image at magnification 2000x, and (d) SEM image at magnification 5000x the damaged chromia layer.

Table 4: EDX spectra analysis of the oxides in different areas for AISI 304 at $T = 1000°C$.

Oxide	Substrate oxides %	Internal oxidation %	External oxidation %
Cr_2O_3	70.57	40.34	6.82
Fe_3O_4	28.54	46.97	—
NiO	0.89	12.69	0.47
Fe_2O_3	—	—	92.71
Total	100.00	100.00	100.00

Table 5: EDX spectra analysis of the oxides in different areas for AISI 316 at $T = 1000°C$.

Oxide	Interior oxides %	Intermediate oxides % (blanket)	External oxides % (blanket)
Cr_2O_3	72.67	41.42	14.18
Fe_3O_4	26.39	32.13	79.21
NiO	1.24	7.91	6.27
MnO	—	18.54	—
Total	100.00	100.00	100.00

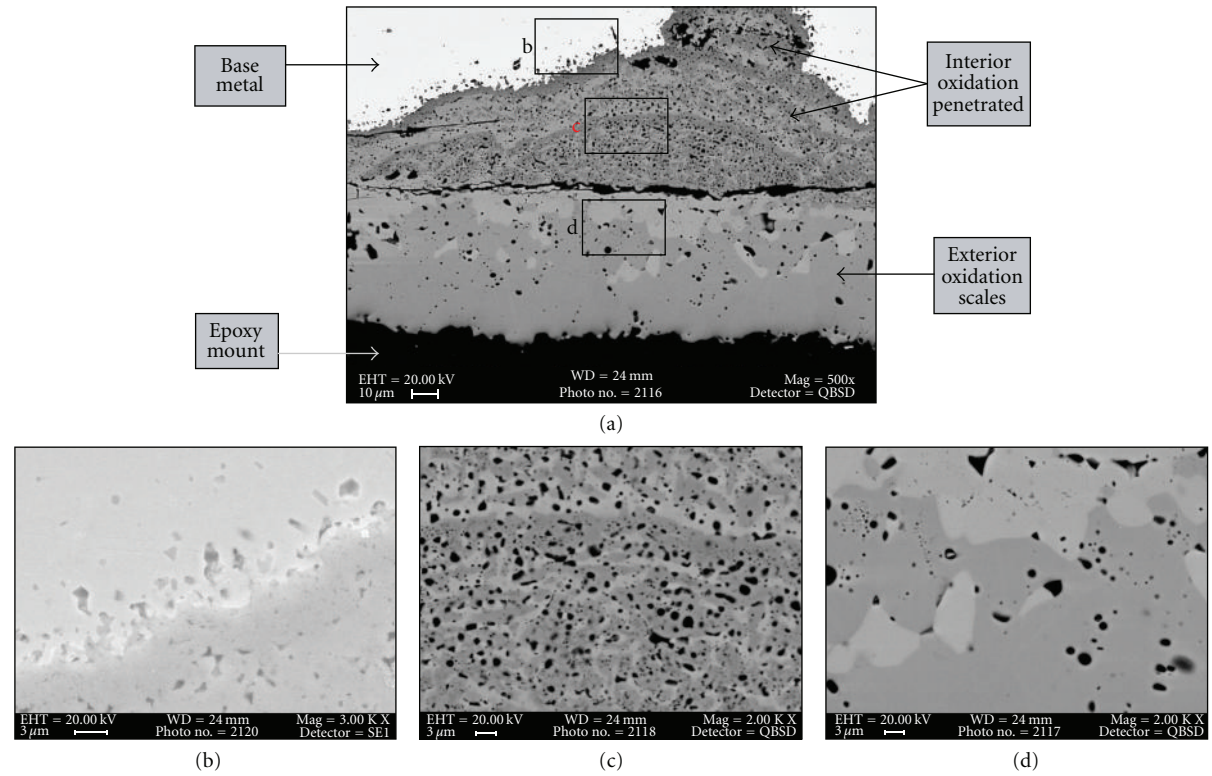

Figure 7: (a) The SEM micrographs of the cross-section of the AISI 304 at 1000°C for 100 hours at magnification 500x, (b) interface substrate-oxide at 3000x, (c) internal oxidation at 3000x, and (d) external oxidation at 2000x.

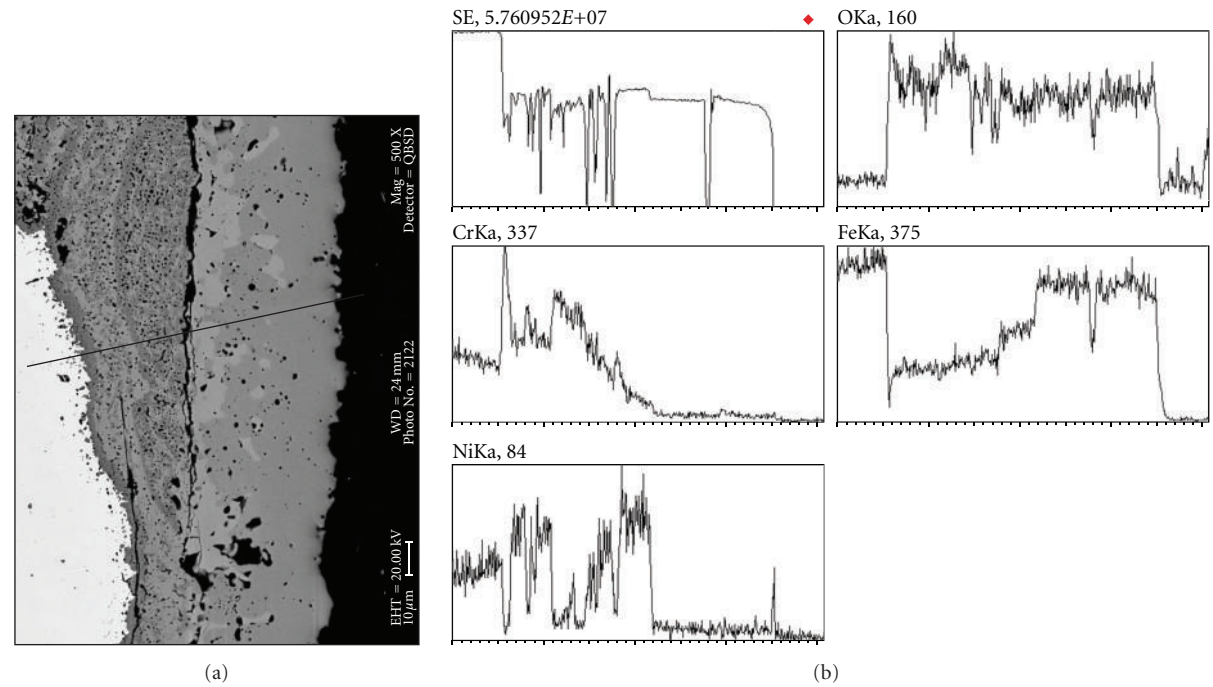

Figure 8: (a) SEM micrograph of the cross-section of the AISI 304 stainless steel oxidized at 1000°C for 100 hours and (b) XRD mapping analysis of the line shown.

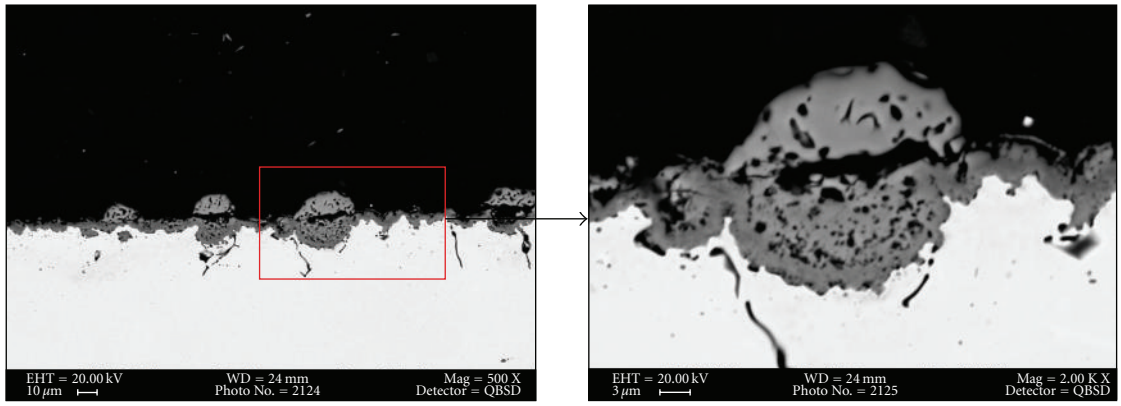

(a) (b)

Figure 9: The SEM micrograph of the cross-section of AISI 316 corroded at $T = 1000^{\circ}C$ in synthetic air at different magnifications: (a) 500x and (b) 2000x.

Figure 9(b) shows pores penetrating under the nodules, which demonstrates less protection of the base metal under each nodule. The interior of the nodule affords a certain protection because the Cr_2O_3 content is high (72.67%) according to the EDX analysis. The intermediate layer of oxides remains adherent to the interior layer of oxides and shows high porosity, even though its Cr_2O_3 content is lower (41.42%); the exterior layer of the nodule is mainly composed of Fe_3O_4 (79.21%) and is separated by a crack in the intermediate layer.

The nodule contour has pores through which oxygen may easily diffuse. EDX microanalysis clearly demonstrates that these nodules are composed mainly of iron oxides, with some manganese. Owing to the large size of these nodules, adherence to the substrate may require an important flux of oxygen [13–15].

The mechanical failure of the initially grown protective layer and codevelopment of several scale phases from the onset of exposure are typical mechanisms that lead to such nodule formation [16–18].

Where nodules did not develop, a continuous oxide scale was observed. The XRD map of this scale shows that it was composed mainly of chromium and it does not seem to be compact and to adhere well to the substrate. This Cr_2O_3 scale would not be able to provide protection to the alloy, which, coupled with the existence of different nodules, may explain the high oxidation rate for the later oxidation times [19, 20].

In conclusion, the breakdown is firstly revealed by the crack in the nodule base and secondly by the poor Cr_2O_3 content of the intermediate and exterior layers of oxides.

Figure 10 shows the X-ray mapping of the elements according to the line chosen to pass through all the oxide scales formed to give a general concept of the diffusion of the elements during the oxidation. The analysis shows an interior oxidation beside the base metal with a continuous, rich Cr_2O_3 layer; also the intermediate and exterior layers show an appreciable content of Cr_2O_3 and Fe_3O_4, which offer some protection. The better behaviour of AISI 316 stainless steel than that of AISI 304 stainless steel regarding the breakdown delay could be explained firstly by the greater content of Cr_2O_3 in all the cross-section layers. Secondly, the exterior layer of AISI 316 stainless steel contains mainly Fe_3O_4, whereas the exterior layer of AISI 304 stainless steel contains Fe_2O_3, which has less protection capacity against oxidation. Finally, the interior and intermediate oxidation layers of AISI 316 stainless steel have greater contents of NiO, which makes cation diffusion through the oxidation layers more difficult.

7. Conclusions

(i) The breakdown of AISI 304 and AISI 316 stainless steels occurred at 1,000°C in synthetic air, after 2 h for AISI 304 stainless steel and after 77 h for AISI 316 stainless steel.

(ii) At 1,000°C in synthetic air and after an exposure time of 100 h, the mass gain of AISI 304 stainless steel was about 8 times greater than that of AISI 316 stainless steel.

(iii) The breakdown of AISI 304 and AISI 316 stainless steels means the Cr_2O_3 protective layer is lost, but the damaging process in both cases is different, especially with regard to the exterior layer of AISI 304 stainless steel, which has totally lost Cr_2O_3 and mainly has Fe_2O_3, whereas the exterior layer of AISI 316 still contains some Cr_2O_3 and mainly has Fe_3O_4.

(iv) The superficial morphologies of the AISI 304 and AISI 316 stainless steels after the breakdown are different; characteristic islands rich in Fe_2O_3 appeared on the outer scale of AISI 304 stainless steel, whereas characteristic nodules rich in Fe_3O_4 appeared on the outer scale of AISI 316 stainless steel.

(v) After breakdown, AISI 304 and AISI 316 stainless steels show three different areas of oxidation in the cross-section, and these have different morphology, thickness, and composition.

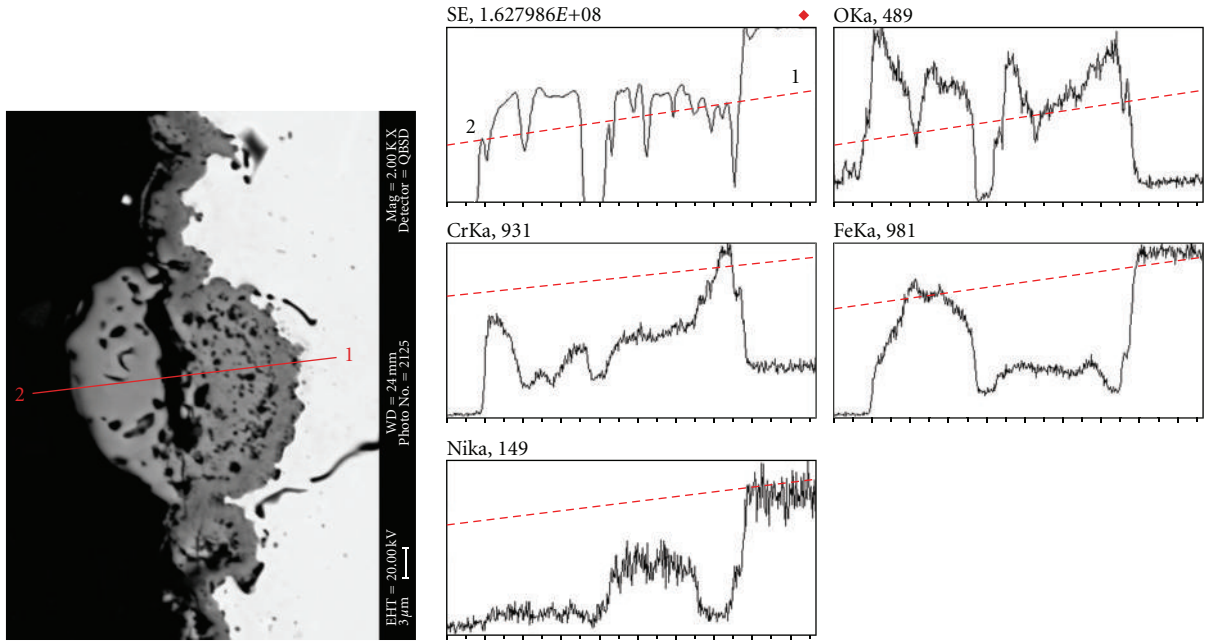

Figure 10: (a) SEM micrograph of the cross-section of the AISI 316 stainless steel oxidized at 1000°C for 100 hours and (b) XRD mapping analysis of the line shown.

Acknowledgments

The authors gratefully acknowledge the financial support provided by Fundació Caixa Castelló-Bancaixa through Grant P1.1A2008-13. Special thanks are due to Jose Ortega and Raquel Oliver, at the Laboratory of Engineering Materials, for their help during the experiments and also to Javier Gomez and Gabriel Peris, from the SCIC at Universitat Jaume I in Castellón.

References

[1] A. J. Sedriks, *Corrosion of Stainless Steels*, John Wiley & Sons, New York, NY, USA, 1996.

[2] A. S. Khanna, *Introduction to High Temperature Oxidation and Corrosion*, ASM International, Materials Park, 2002.

[3] G. Y. Lai, *High-Temperature Corrosion of Engineering Alloys*, ASM International, Materials Park, 1990.

[4] M. Schutze, *Protective Oxide Scales and Their Breakdown*, Institute of Corrosion and Wiley Series on Corrosion and Protection, John Wiley & Sons, Chichester, UK, 1997.

[5] G. W. Meetham and M. H. Van de Voorde, *Materials for High Temperature Engineering Applications*, Springer, Berlin, Germany, 2000.

[6] H. Asteman, J.-E. Svensson, and L.-G. Johansson, "Evidence for chromium evaporation influencing the oxidation of 304L: the effect of temperature and flow rate," *Oxidation of Metals*, vol. 57, no. 3-4, pp. 193–216, 2002.

[7] N. Otsuka, Y. Nishiyama, and T. Kudo, "Breakaway oxidation of TP310S stainless-steel foil initiated by Cr depletion of the entire specimen in a simulated flue-gas atmosphere," *Oxidation of Metals*, vol. 62, no. 1-2, pp. 121–139, 2004.

[8] M. S. Damra, *High Temperature Corrosion of Stainless Steels and NiCrAlY Superalloy Coatings Deposited by Oxyfuel Thermal Spraying Technique*, Ph.D. thesis, Universitat Jaume I, Castellón, Spain, 2009.

[9] F. J. Pérez, F. Pedraza, M. P. Hierro, J. Balmain, and G. Bonnet, "Comparison of the high-temperature oxidation of uncoated and CVD-FBR aluminized AISI-304 stainless steel," *Oxidation of Metals*, vol. 58, no. 5-6, pp. 563–587, 2002.

[10] N. S. Quan and D. J. Young, "Sulfidation behavior of an aluminum-manganese steel," *Oxidation of Metals*, vol. 25, no. 1-2, pp. 107–119, 1986.

[11] B. Pieraggi, "Calculations of parabolic reaction rate constants," *Oxidation of Metals*, vol. 27, no. 3-4, pp. 177–185, 1987.

[12] H. Hindam and D. P. Whittle, "Microstructure, adhesion and growth kinetics of protective scales on metals and alloys," *Oxidation of Metals*, vol. 18, no. 5-6, pp. 245–284, 1982.

[13] G. Aguilar, *Oxydation isotherme et cyclique de deux alliages métalliques: influence d'un dépot d'oxyde de cerium*, Ph.D. thesis, Université de Bourgogne, Dijon, France, 1991.

[14] E. Otero, F. J. Pérez, M. P. Hierro et al., "High temperature corrosion protection of austenitic AISI 304 stainless steel by Si, Mo and Ce ion implantation," *Surface and Coatings Technology*, vol. 108-109, no. 1–3, pp. 127–131, 1998.

[15] J. Stringer, "Coatings in the electricity supply industry: past, present, and opportunities for the future," *Surface and Coatings Technology*, vol. 108-109, pp. 1–9, 1998.

[16] F. J. Pérez, F. Pedraza, M. P. Hierro, M. C. Carpintero, C. Gómez, and R. Tar Ín, "Effect of fluidized bed CVD aluminide coatings on the cyclic oxidation of austenitic AISI 304 stainless steel," *Surface and Coatings Technology*, vol. 145, no. 1–3, pp. 1–7, 2001.

[17] T. F. An, H. R. Guan, X. F. Sun, and Z. Q. Hu, "Effect of the θ-α-Al_2O_3 transformation in scales on the oxidation behavior of a nickel-base superalloy with an aluminide diffusion coating," *Oxidation of Metals*, vol. 54, no. 3-4, pp. 301–316, 2000.

[18] F. H. Stott, G. C. Wood, and J. Stringer, "The influence of alloying elements on the development and maintenance of protective scales," *Oxidation of Metals*, vol. 44, no. 1-2, pp. 113–145, 1995.

[19] S. C. Tsai, A. M. Huntz, and C. Dolin, "Growth mechanism of Cr_2O_3 scales: oxygen and chromium diffusion, oxidation kinetics and effect of yttrium," *Materials Science and Engineering A*, vol. 212, no. 1, pp. 6–13, 1996.

[20] P. Tomaszewicz and G. R. Wallwork, "Observations of nodule growth during the oxidation of pure binary iron-aluminum alloys," *Oxidation of Metals*, vol. 19, no. 5-6, pp. 165–185, 1983.